

Basal cell adenoma of the parotid gland;
MR features and differentiation from
pleomorphic adenoma

(耳下腺基底細胞腺腫：MRI所見と多形
腺腫との鑑別)

千葉大学大学院医学薬学府
先端医学薬学専攻
(主任：宇野隆教授)
向井 宏樹

Abstract

Objectives

Among benign tumours of the parotid gland, basal cell adenoma (BCA) is far less common than pleomorphic adenoma (PA). Magnetic resonance (MR) features of BCA, including diffusion-weighted imaging and dynamic contrast-enhanced study, have not been previously described. Assessment of the crucial MR features of BCA appears to offer beneficial clues for distinguishing BCA from PA.

Methods

We retrospectively reviewed 14 BCAs and 179 PAs in the parotid gland, collected between March 2000 and May 2012, from the MR imaging database..

Results

Nearly half of the BCAs had cystic components. The average ratio of the maximum diameter of the cysts to the BCAs (cystic ratio) was 0.80 ± 0.11 [standard deviation(SD)]. The BCA cystic ratio was significantly higher ($p=0.00232$) than that of PAs. The cystic ratio threshold was 0.65 between cystic BCA and cystic PA. Sensitivity and specificity were 76.5% and 100%, respectively. The average of the apparent diffusion coefficient (ADC) values of the 12 BCAs (1.24 ± 0.18 [SD] $\times 10^{-3} \text{mm}^2/\text{sec}$) was significantly lower than that of the 151 PAs (1.86 ± 0.40 [SD] $\times 10^{-3} \text{mm}^2/\text{sec}$) ($p<0.001$) and also that of the cystic PAs (1.83 ± 0.57 [SD] $\times 10^{-3} \text{mm}^2/\text{sec}$) ($p=0.00495$). The ADC threshold was $1.31 \times 10^{-3} \text{mm}^2/\text{sec}$ between BCA and cystic PA, with sensitivity and specificity of 81.2% and 91.7%, respectively, and also the same $1.31 \times 10^{-3} \text{mm}^2/\text{sec}$ between BCA and PA, with sensitivity and specificity of 92.7% and 91.7%, respectively. Time–signal intensity curves (TICs) showed various patterns.

Conclusions

Small cystic mass with well-circumscribed borders and slightly lower ADC value may suggest BCA, although TICs showed various patterns.

Introduction

By the previous WHO classification (1991), basal cell adenoma (BCA) was recognized as an independent entity among salivary gland tumours. Although the incidence of BCA is 1-7.5%, it is the third most common type of benign parotid tumour [1, 2]. BCA predominantly affects persons over 50 years of age and is seen more often in females. Most BCAs are unilateral and round or oval in shape with well-circumscribed borders, and they are usually less than 3.0 cm in diameter in the superficial lobe of the parotid gland at the time of excision. A painless, slowly enlarging mass is the most common clinical symptom. Some surgeons have mistaken these tumours for lymph nodes clinically. The accuracy of the cytological diagnosis of BCA is not so good [3]. The majority of BCAs arise in the major glands, with the parotid gland being the most frequent site. BCAs are composed of basaloid cells with eosinophilic cytoplasm, have indistinct cell borders and round to oval nuclei, and are distributed in solid, trabecular, tubular, and membranous patterns [4]. However, the tumours may present with more than one of these patterns, although one will usually predominate. Membranous BCA has biologic behavior different from that of the other variants of BCA in that it has multifocal microadenomas, incomplete or no capsules, frequent postoperative recurrences, and malignant transformations [4].

Pleomorphic adenoma (PA) is the most common benign neoplasm of parotid gland origin, being the most common neoplasm of the salivary gland even in children

and adolescents [5]. Women are more likely to be affected than men. PA is usually solitary, round, and well-circumscribed, with a smooth but sometimes lobulated surface. Tumours larger than 1-cm diameter often have numerous protuberances, giving them a lobulated appearance. PAs are commonly encapsulated in parotid glands. PAs are renowned for their cytomorphological and architectural variability. Despite their protean histopathology, all tumours share the essential diagnostic features of being composed of both epithelial and myxoid tissues [5]. The proportions of these components vary widely, although one or the other is often predominant. The variety of magnetic resonance (MR) findings of PAs reflects their cytomorphological and architectural variability [6]. The diagnostic clue of PA is to find the myxoid component, which shows high intensity on short-inversion-time inversion recovery (STIR) and T2-weighted images, progressive enhancement on dynamic MR images, and high apparent diffusion coefficient (ADC) values on diffusion-weighted (DW) images [6].

Warthin's tumour (WT) is the second most common type of benign parotid tumour. Its incidence is markedly higher in elderly males and most tumours develop in the inferior pole of the parotid gland [7]. The features of WT are different from those of PA [8]. Typical WT shows early enhancement and high washout ratio on dynamic enhanced study, and low ADC value on DW images [8].

Of course, clinicians want to know first whether a parotid gland tumour is malignant or benign. If it is the former, they want to know whether it is low- or high-grade malignancy. However, if it is benign, they want to know whether it is PA tending to recur, or others. Surgical treatment for PA is a complete, wide surgical excision with a good safety margin, and inadequate resection or rupture of the capsule

or tumour spillage during excision can lead to local recurrence. WT undergoes local excision, as there is no worry about the margin. As for BCA, the prognosis is good except for the membranous type. The recurrence rate is so low as to be almost non-existent, especially when conservatively but adequately excised. If it is possible to show the BCA on MRI to the clinician, it will provide useful information.

There are few reports regarding MR imaging findings of BCAs, and especially any including dynamic enhanced study and ADC values [9-13]. The present study aimed to describe the MR features of BCAs and to clarify the differences between BCAs and PAs.

Materials and Methods

Patients

We retrospectively reviewed 14 BCAs (5 men and 9 women; median 52 years, range 39-75 years) and 179 PAs (51 men and 128 women; median 48 years, range 16-84 years) in the parotid gland, collected between March 2000 and April 2012 from the MR imaging database of our hospital.

MR Imaging Techniques

All MRI examinations were performed using 1.5-T MRI units (GE Medical Systems, Milwaukee, WI, USA) with a neurovascular array coil. T1-weighted images (400-560/8-14 [repetition time msec./echo time msec.]) of the transverse plane, STIR images (3000-4000/30-40, 12 [echo train length], 150 [inversion time msec.]) of the same transverse plane as the T1-weighted images, DW images (spin-echo single-shot echo-planar sequence with b factors of 0 and 1,000 sec/mm²) of the same transverse plane, and T2-weighted SE images (4000/104, 16 [echo train length]) of the coronal

plane were obtained at a section thickness of 6 mm, an intersection gap of 1 mm, an acquisition matrix of 256 x 256, and a field of view (FOV) of 22 x 22 cm.

Dynamic contrast-enhanced MR images were obtained by three-dimensional fat suppression T1-weighted multiphase spoiled gradient-recalled-echo (SPGR) (6.3/1.5 [repetition time msec./echo time msec.]) for 4 min, with each phase lasting 27 sec followed by a 3-sec interval, an effective section thickness of 4 mm, a FOV of 22 x 22 cm, and an acquisition matrix of 256 x 256. After the first set was obtained, contrast material injection was started immediately. Gadodiamide hydrate was administered (0.2 ml/kg body weight) at a rate of 2.0 ml/sec followed by a 20-ml saline flush into the antecubital vein. Seven sets of dynamic contrast-enhanced images were obtained serially at 3, 33, 63, 93, 123, 153, and 183 sec. Soon after the dynamic contrast-enhanced MR imaging, fat suppression T1-weighted images (340-400/20 [repetition time msec./echo time msec.]) of the same transverse plane as the pre-contrast enhanced T1-weighted images were obtained. Apparent diffusion coefficient (ADC) maps were automatically constructed from DW images.

Image and Pathological Analysis

All MR images were retrospectively evaluated with respect to size, location, marginal morphology (definition and lobulation), and enhancement behavior by 2 experienced radiologists (H.M and K.M). The signal intensities of the lesions on each dynamic image were measured with an electronic cursor to define the region of interest (ROI) in each patient. Where markedly heterogeneous enhancement was seen, multiple ROIs were obtained. When measuring the signal intensities, obvious cystic portions were avoided. Time–signal intensity curves (TICs) of the solid components of the lesions on dynamic MRIs were plotted, and washout ratios were

also calculated. TICs were divided into 3 types: Type A, curve peaks earlier than 120 sec (<120 sec) after administration of contrast material with a high washout ratio (>30%); Type B, curve peaks earlier than 120 sec (<120 sec) with a low washout ratio (<30%); Type C, curve peaks later than 120 sec (>120 sec) [14].

The ADC values of the lesions were measured on each DW image with an electronic cursor to define the ROI. When measuring the signal intensities, obvious cystic portions were avoided.

Statistical Analysis

Mann-Whitney U test was used to compare the size and ADC values of BCAs and PAs. The optimal cutoff values for the cystic ratio and ADC value were calculated by means of receiver operating characteristic (ROC) analysis for distinguishing between BCAs and PAs. All statistical analyses were performed with EZR (Saitama Medical Center, Jichi Medical University), which is a graphical user interface for R (The R Foundation for Statistical Computing, version 2.13.0) [15].

Results

MR Imaging Findings

Size, Location, and Marginal Morphology

The average maximal cross-sectional diameter of 14 BCAs was 2.7 ± 0.77 cm [SD] (1.5 - 4.4 cm). Twelve BCAs (86%) were located in the superficial lobe of the parotid gland and the other 2 (14%) in the deep lobe. All BCAs showed well-defined margins, and 4 tumours (29%) had lobulated margins. Six of the 14 BCAs (43%) had cystic components. The average maximal diameter of the cysts was 2.3 ± 0.96 cm [SD] and the average ratio of the maximum diameter of the cysts to the

tumours (cystic ratio) was 0.80 ± 0.11 [SD] (0.65-0.90).

The average maximal cross-sectional diameter of 179 PAs was 2.8 ± 1.3 cm [SD] (0.7 – 11 cm). One hundred and sixty-two PAs (91%) were located in the superficial lobe of the parotid gland and the other 17 (9%) in the deep lobe. Seventeen of the 179 PAs (9%) had cystic components. The average maximal diameter of the cysts was 1.7 ± 0.80 cm [SD] and the cystic ratio was 0.48 ± 0.21 [SD] (0.20-0.88).

There was no significant difference between BCAs and PAs in maximal cross-sectional diameter. The cystic ratio of the BCAs was significantly higher than that of the PAs ($p=0.00232$). The cystic ratio threshold derived from the ROC curve-based positive test was 0.65 between cystic BCA and cystic PA. Sensitivity and specificity were 76.5% and 100%, respectively.

ADC Values of Tumours

DW images were obtained from 12 of the 14 BCAs and 151 of the 179 PAs, and the ADC values of the tumours were calculated. The average of the ADC values of the 12 BCAs (1.24 ± 0.18 [SD], 0.74 to $1.50 \times 10^{-3} \text{mm}^2/\text{sec}$) was significantly lower than that of the 151 PAs (1.86 ± 0.40 [SD], 1.09 to $2.86 \times 10^{-3} \text{mm}^2/\text{sec}$) ($p<0.001$) and also that of the cystic PAs (1.83 ± 0.57 [SD], 1.09 to $2.86 \times 10^{-3} \text{mm}^2/\text{sec}$) ($p=0.00495$). The ADC thresholds derived from the ROC curve-based positive test were $1.31 \times 10^{-3} \text{mm}^2/\text{sec}$ between BCA and PA, with sensitivity and specificity of 92.7% and 91.7%, respectively.

Time-versus-contrast Enhancement Ratio and Washout Ratio of Tumours

Two of the 14 (14%) BCAs had type A curve, 2 (14%) had type B curves, 5 (36%) had type B and C curves, and 5 (36%) had type C curves. Three of the 17

cystic PAs (18%) had type B curves, 2 (12%) had type B and C curves, and 12 (70%) had type C curves. Comparison of the imaging features between BCAs and PAs are summarized in Table 1.

Correlations between Radiological and Pathological Findings

All BCAs had fibrous capsules at the maximal diameter section. Ten of the BCAs were classified as trabecular dominant type, one as tubular dominant type, and three as solid dominant type. Twelve BCAs existed in the superficial lobe and 2 in the deep lobe. Cystic changes were seen in 6 tumours, 5 of which were in the superficial lobe and 1 in the deep lobe. Large fibrous scars were seen in 2 BCAs and small fibrous scars in 4. Cystic degeneration was seen in 6 BCAs. All BCAs had many vascular channels. Subtypes, ADC values, TICs, and washout ratio of the tumours are summarized in Table 2.

In Case 10 (Fig. 1), the tumour in the superficial lobe of the left parotid gland had a solid component showing type B enhancement and a large cyst. The cystic ratio was 0.68. The pathological specimen revealed the trabecular type of BCA, with anastomosing cords of basaloid cells and intervening stroma.

In Case 11 (Fig. 2), the tumour in the deep lobe of the right parotid gland showed type C enhancement and had an ADC value of $1.31 \times 10^{-3} \text{mm}^2/\text{sec}$. The pathological specimen revealed the trabecular type of BCA, with rich intervening stroma.

In comparative images of cystic PA (Fig. 3), the tumour in the deep lobe of the right parotid gland showed type C enhancement and had an ADC value of $1.52 \times 10^{-3} \text{mm}^2/\text{sec}$. The cystic ratio was 0.22. Cystic PA had smaller cystic ratio and higher ADC value than BCA. TIC curve of cystic PA was type C as shown

in some BCA.

Discussion

In this study, the median age of BCA patients was 52 years. All BCAs were unilateral and had well-circumscribed borders. A painless, slowly enlarging mass was the usual clinical symptom. The average maximal cross-sectional diameter of the 14 BCAs was 2.7 ± 0.77 cm [SD]. Our data agreed well with those of previous articles. Four of the 14 BCAs (29%) had lobulated margins in this study. Generally, a lobulated appearance is a particular feature of PA when it is larger than 1 cm.

According to Shi et al [10], BCA in the superficial region tends to be solid and small in size. Cystic BCAs occur mostly in the deeper region. This trend was not observed in our study, but 6 of the 14 BCAs (43%) had cystic components. On the other hand, only 17 of the 179 PAs (9%) showed cystic degeneration in our study. The cystic ratio of the BCAs was significantly higher than that of the PAs ($p=0.00232$), and the cystic ratio threshold was 0.65 between cystic BCA and cystic PA.

Some MR imaging findings of BCAs of the parotid gland have been reported [11-13], but those reports have not included DW images, ADC values, and TICs with washout ratio. MR imaging findings of basal cell adenomas are relatively low signal intensities on T1-weighted images and hypointense to slightly hyperintense on T2-weighted images, showing rapid and prolonged enhancement on dynamic study. BCA sometimes has cystic or hemorrhagic components. In fact, it is difficult to make a differential diagnosis between BCA and PA from only the slight difference in the signal intensities on T1-weighted and T2-weighted images. In our study, in 9 of the 14 BCAs (64%), 2 had type A, and 7 had type B curves on dynamic enhanced study,

with rapidly enhanced components. Ten of the 14 BCAs (71%) had gradual upward enhanced components. According to past articles of parotid tumours, the types of TICs at gadolinium-enhanced dynamic MR imaging correlate well with histopathologic findings. Rapid enhancement and high washout ratio (type A) for Warthin's tumours, low washout ratio (type B) for malignant tumours, and gradual upward enhancement (type C) for pleomorphic adenomas were observed in most instances. In our study, 7 of the 14 BCAs (50%) had malignant type of TIC (type B) at gadolinium-enhanced dynamic MR imaging. Tumour cells, vascular channels, ductal lumen, stroma, and fibrosis were mixed at various proportions in the BCAs. These various proportions resulted in a variety of TICs on dynamic MR images: type A, cellular component-dominant area showing early enhancement and high washout ratio; type B, cellular components with moderate stroma and fibrosis showing early enhancement with poor washout; type C, abundant stroma or fibrotic tissue with few cellular components showing gradual upward enhancement. Our study also reports the ADC values on diffusion-weighted images in patients with BCA. The average of the ADC values of the BCAs (1.24 ± 0.18 [SD] $\times 10^{-3} \text{mm}^2/\text{sec}$) was significantly lower than that of the PAs (1.86 ± 0.40 [SD] $\times 10^{-3} \text{mm}^2/\text{sec}$). The ADC threshold was $1.31 \times 10^{-3} \text{mm}^2/\text{sec}$ between BA and PA. There is no report of specific ADC value of BCA, although Yerli showed that ADC value of adenomas including 6 PA and 2 BCA was $1.75 \pm 0.40 \times 10^{-3} \text{mm}^2/\text{sec}$ [16]. Our result of ADC value on PA and BCA seems to be compatible with the previous report. A previous article reported an ADC threshold of 1.22, or $1.40 \times 10^{-3} \text{mm}^2/\text{sec}$ between malignancy and PA. The ADC value of BCA in our study was between 0.74 and $1.50 \times 10^{-3} \text{mm}^2/\text{sec}$. According to the threshold level of $1.40 \times 10^{-3} \text{mm}^2/\text{sec}$ [17], all BCAs except for Case 12 in our

study might be classified as malignant tumours. All BCAs had well-defined margins suggesting benign tumours morphologically, which indicates a discrepancy with the results of TIC and ADC analysis. Because BCA is a relatively rare benign epithelial tumour, past MR study of salivary gland tumours did not include BCAs [17]. The BCAs in our study had fibrous capsules, with many of them having fibrous scars and cystic degeneration. All BCAs also had many vascular channels. Clear margins as benign and TICs as malignant or PA may reflect these pathological features.

Although the ADC values and TICs may classify BCA as malignant according to past study [17], the morphological features of a clear margin and relatively small size, less than 3.0 cm in diameter, suggest BCA as being benign. Large cystic ratio and slightly lower ADC value are clues for differentiating BCA and PA.

Our study has some limitations. First, this study had a relatively small number of BCA. We had no membranous-type BCA and most of our cases consisted of trabecular type. Thus, our study population might not make a satisfactory assessment of the correlation between pathological types and MR results. Further studies in more patients are needed. Second, manual ROI setting to measure TIC and ADC value is a subjective method. However, the ROI method is the most common method in previous papers [6, 8, 14, 17]. We set ROIs as carefully as possible to maintain consistency among TIC, ADC value and pathological features.

In conclusion, BCA predominantly affected older persons (> 50 years) and occurred more often in females. A painless, slowly enlarging mass was the main clinical symptom. All BCAs (except membranous type) were unilateral small masses, usually less than 3.0 cm in diameter, with well-circumscribed borders. BCA often had a cystic component, and the ratio of the maximum diameter of the cysts to the

tumours in BCA was significantly higher than that in PA. The cystic ratio threshold was 0.65 between cystic BCA and cystic PA. The ADC values of BCA (1.24 ± 0.17 [SD], 0.74 to $1.50 \times 10^{-3} \text{mm}^2/\text{sec}$) were significantly lower than those of PA. Cystic small mass with well-circumscribed borders and slightly lower ADC value may suggest BCA regardless of the TIC pattern.

References

1. Takahashi H, Fujita S, Okabe H, Tsuda N, Tezuka F. Immunohistochemical characterization of basal cell adenomas of the salivary gland. *Pathol Res Pract* 1991; 187: 145-56
2. Nagao K, Matsuzaki O, Saiga H, Sugano I, Shigematsu H, Kaneko T, et al. Histopathologic studies of basal cell adenoma of the parotid gland. *Cancer* 1982; 50: 736-45
3. Kawahara A, Harada H, Akiba J, Yokoyama T, Kage M. Fine-needle aspiration cytology of basal cell adenoma of the parotid gland: characteristic cytological features and diagnostic pitfalls. *Diagn Cytopathol* 2007; 35: 85-90.
4. De Araujo VC. Basal cell adenoma. In: L Barnes, JW Everson, P Reichart, D Sidransky, editor. World Health Organization classification of tumours: pathology and genetics of the head and neck tumours. IARC press, Lyon; 2005: 261-2
5. JW Eveson, K Kusafuka, G Stenman, T Nagao. Pleomorphic adenoma. In: L Barnes, JW Everson, P Reichart, D Sidransky, editor. World Health Organization classification of tumours: pathology and genetics of the head and neck tumours. IARC press, Lyon; 2005: 254-8
6. Motoori K, Yamamoto S, Ueda T, Nakano K, Muto T, Nagai Y, et al. Inter- and

- intratumoral variability in magnetic resonance imaging of pleomorphic adenoma: an attempt to interpret the variable magnetic resonance findings. *J Comput Assist Tomogr* 2004; 28: 233-46
7. Simpson RHW, Eveson JW. Warthin tumor. In: L Barnes, JW Everson, P Reichart, D Sidransky, editor. World Health Organization classification of tumours: pathology and genetics of the head and neck tumours. IARC press, Lyon; 2005: 263-5
 8. Ikeda M, Motoori K, Hanazawa T, Nagai Y, Yamamoto S, Ueda T, et al. Warthin Tumor of the Parotid Gland: Diagnostic Value of MR Imaging with Histopathologic Correlation. *AJNR Am J Neuroradiol* 2004; 25: 1256-62
 9. NC Chiu, HM Wu, YH Chou, WY Li, YY Chiou, WY Guo, et al. Basal cell adenoma versus pleomorphic adenoma of the parotid gland: CT findings. *AJR Am J Roentgenol* 2007; 189: 254-61
 10. L Shi, YXJ Wang, C Yu, F Zao, PD Kuang, GL Shao. CT and ultrasound features of basal cell adenoma of the parotid gland: a report of 22 cases with pathologic correlation. *AJNR Am J Neuroradiol* 2012; 33: 434-8
 11. H Yerli, M Teksam, E Aydin, M Coskun, H Ozdemir, AM Agildere. Basal cell adenoma of the parotid gland: dynamic CT and MRI findings. *Br J Radiol* 2005; 78: 642-5
 12. Okahara M, Kiyosue H, Matsumoto S, Hori Y, Tanoue S, Uchida D, et al. Basal cell adenoma of the parotid gland: MR Imaging Findings with Pathologic Correlation. *AJNR Am J Neuroradiol* 2006; 27: 700-4
 13. Kawata R, Yoshimura K, Lee K, Araki M, Takenaka H, Tsuji M. Basal cell adenoma of the parotid gland: a clinicopathological study of nine cases- basal

cell adenoma versus pleomorphic adenoma and Warthin's tumor. *Eur Arch Otorhinolaryngol* 2010; 267: 779-83

14. Yabuuchi H, Fukuya T, Tajima T, Hachitanda Y, Tomita K, Koga M. Salivary Gland Tumors: Diagnostic Value of Gadolinium-enhanced Dynamic MR Imaging with Histopathologic Correlation. *Radiology* 2003; 226: 345-54
15. Kanda Y. Investigation of the freely-available easy-to-use software "EZR"(Easy R) for medical statistics. *Bone Marrow Transplant*. 2013;48,452-458. Advance online publication 3 December 2012; doi: 10.1038/bmt.2012.244
16. H Yerli, E Aydin, N Haberal, A Harman, T Kaskati, S Alibek. Diagnosing common parotid tumours with magnetic resonance imaging including diffusion-weighted imaging vs fine-needle aspiration cytology: a comparative study. *Dentomaxillofacial Radiology* 2010; 39: 349-355
17. Yabuuchi H, Matsuo Y, Kamitani T, Setoguchi T, Okafuji T, Soeda H, et al. Parotid gland tumors: can addition of diffusion-weighted MR imaging to dynamic contrast-enhanced MR imaging improve diagnostic accuracy in characterization? *Radiology* 2008; 249: 909-16

Table 1**Comparison of imaging features between BCAs and PAs**

MR findings	BCAs	PAs	p value
Diameter of the tumours (cm)	2.7±0.77(1.5-4.4)	2.8±1.3(0.7-11)	0.88993
Tumour site*	86 %	91 %	
Cystic components	43 %(6/14)	9 %(17/179)	
Diameter of the cysts (cm)	2.3±0.96	1.7±0.8	
Cystic ratio	0.80±0.11	0.48±0.21	
TICs	type A 14 % type B 14 % type C 36 % type B+C 36 %	type B 18 % type C 70 % type B+C 12 %	
ADC values(x10 ⁻³ mm ² /sec)	1.24±0.18(0.74-1.50)	1.86±0.40(1.09-2.86)	<0.001
		1.83±0.57(1.09-2.86):cystic PAs	0.00495

*Ratios for the superficial lobe tumour

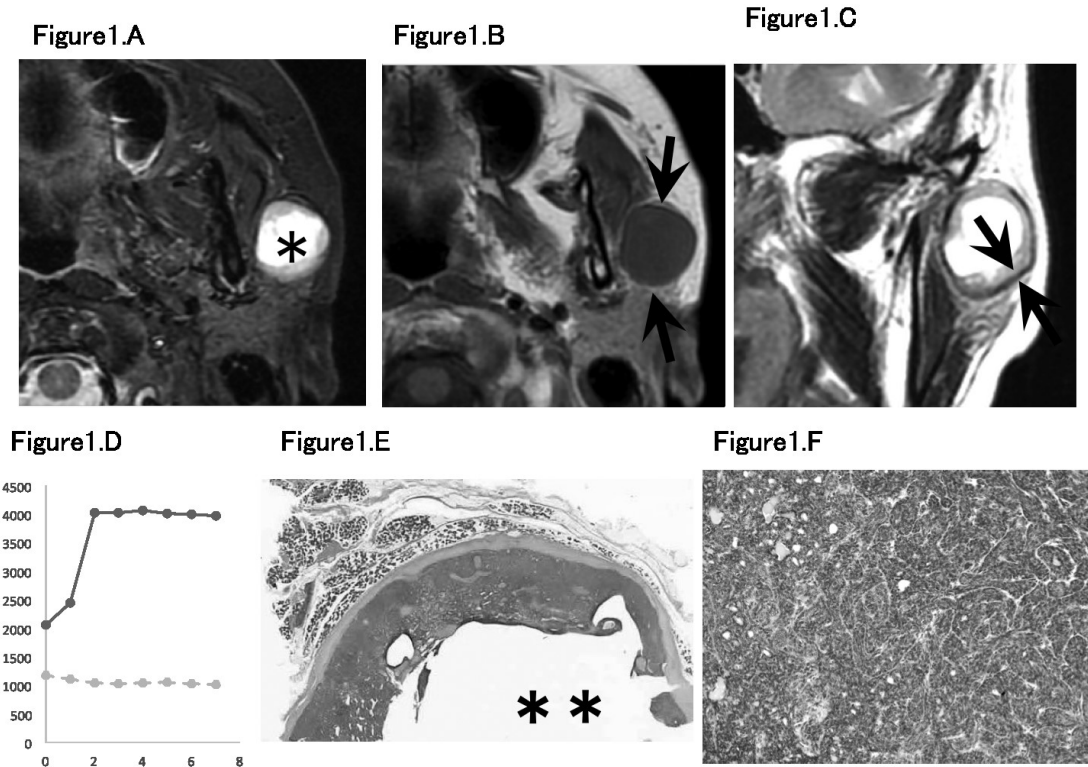
Table 2**Clinical and imaging features of BCA**

Case	Age	Sex	Tumour size (cm)	Cyst size (cm)	Cystic ratio	ADC value (x10 ⁻³ mm ² /sec)	TICs type	Tumour site
#1	53	F	2.9	2.6	0.90	-	B, C	S
#2	60	F	2.1	1.7	0.81	-	C	S
#3	67	M	2.8	2.5	0.89	1.25	B	S
#4	40	F	2.1	-	-	1.22	C	S
#5	42	M	3.0	-	-	1.29	B, C	S
#6	61	F	1.7	1.2	0.65	1.23	A	S
#7	51	F	3.7	-	-	1.30	B, C	S
#8	41	M	2.8	-	-	1.23	B, C	S
#9	39	M	4.4	3.9	0.89	1.25	C	D
#10	56	F	2.6	1.8	0.68	1.28	B	S
#11	49	F	2.3	-	-	1.31	C	D
#12	75	F	4.4	-	-	1.50	B, C	S
#13	43	F	2.6	-	-	0.74	C	S
#14	68	M	2.3	-	-	1.29	A	S

F female, *M* male, *S* superficial lobe tumour, *D* deep lobe tumour

Figures

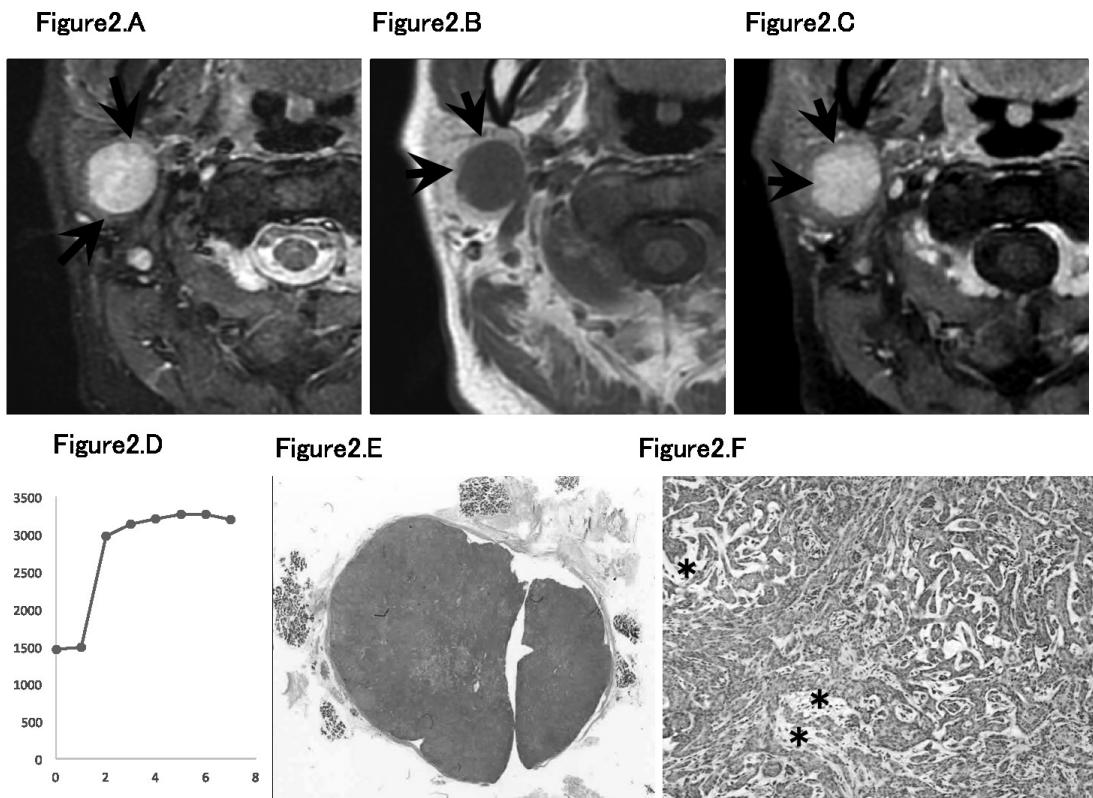
Figure 1



BCA in the left parotid gland of a 56-year-old female. **A**, STIR image (3000/40 [TR/TE], axial plane) shows a superficial lobe tumour with moderately high intensity in the peripheral region and markedly high intensity in the central area (*). The markedly high intensity area is a cystic lesion. **B**, T1-weighted image (560/8, axial plane) shows a hypo-intensity tumour (arrows). **C**, T2-weighted image (4000/104, coronal plane) shows a low intensity capsule around the tumour (arrows). The ratio of the maximum diameter of the cyst to this tumour (cystic ratio) is 0.68. **D**, On axial dynamic enhanced study, TIC of the solid component of this tumour (solid line) shows type B early enhancement with poor washout ratio (4%). The cystic region (dashed line) shows no enhancement. The ADC value of the solid component is

1.28x 10⁻³ mm²/sec. **E**, Loupe image on axial section of the specimen with hematoxylin-eosin (HE) staining shows solid and large cystic components (**). The large cyst had lost its contents. **F**, Solid component has anastomosing cords of basaloid cells and a small amount of intervening stroma (x100 HE staining).

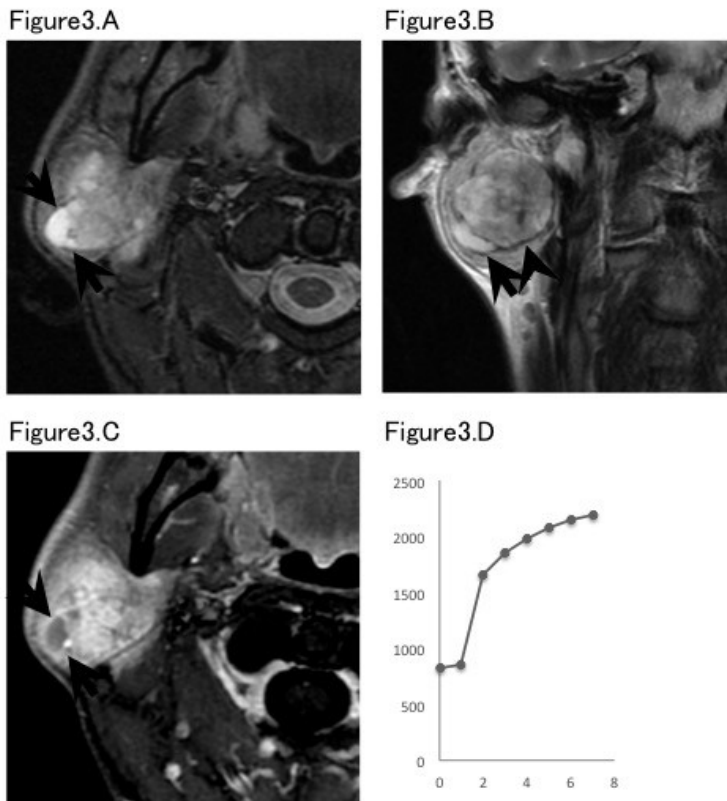
Figure 2



BCA in the right parotid gland of a 49-year-old female. **A**, On STIR image (3000/40 [TR/TE], axial plane), the deep lobe tumour shows heterogeneous high intensities (arrows). **B**, On T1-weighted image (560/8, axial plane), the tumour shows iso-intensity for muscle (arrows). The ADC value of the tumour component is 1.28x 10⁻³ mm²/sec. **C and D**, Fat suppression contrast enhanced T1-weighted image (540/8.2, axial plane) and TIC on enhanced dynamic study, with the tumour showing heterogeneous enhancement (arrows) with TIC curve peaks later than 120 sec (type

C). **E and F**, Loupe and light microscopy (original magnification, x100) images show the solid component with anastomosing cords of basaloid cells and rich intervening stroma (**).

Figure 3



Cystic PA in the right parotid gland of a 37-year-old male. **A**, On STIR image (3000/40 [TR/TE], axial plane), the deep lobe tumour shows heterogeneous moderately high intensities with cystic component in the peripheral region (arrows). **B**, T2-weighted image (4000/104, coronal plane) shows a low intensity capsule (arrowhead). The cystic component is located in the peripheral region (arrow). The cystic ratio is 0.22. **C and D**, Fat suppression contrast enhanced T1-weighted image (540/8.2, axial plane) and TIC on enhanced dynamic study, with the tumour showing heterogeneous enhancement and type C TIC curve. The cystic component has no

enhancement (arrows). The ADC value of the solid component was 1.52×10^{-3} mm²/sec.

Dentomaxillofacial Radiology (2016) 45, 20150322

平成28年2月3日 公表済